Enhancement of the Leaching Rate of Uranium in the Presence of Ultrasound

ARTICLE *in* INDUSTRIAL & ENGINEERING CHEMISTRY RESEARCH · SEPTEMBER 2006

Impact Factor: 2.59 · DOI: 10.1021/ie060599x

5 AUTHORS, INCLUDING:

Avvaru Balasubrahmanyam
Institute of Chemical Technology, Mumbai
7 PUBLICATIONS **135** CITATIONS

SEE PROFILE

Aniruddha Pandit
Institute of Chemical Technology, Mumbai
320 PUBLICATIONS **9,150** CITATIONS

SEE PROFILE

Enhancement of the Leaching Rate of Uranium in the Presence of Ultrasound

Balasubrahmanyam Avvaru,[†] S. B. Roy,[‡] Sujit Chowdhury,[‡] K. N. Hareendran,[‡] and Aniruddha B. Pandit*,[†]

Chemical Engineering Division, Institute of Chemical Technology, Matunga, Mumbai, India, and Uranium Extraction Division, Bhabha Atomic Research Center (BARC), Mumbai, India

In the present work, experiments have been performed for leaching (recovery) of uranium from MgF_2 (byproduct from the uranium ore recovery process) under various conditions of leach acid concentration with and without the presence of ultrasound, under different energy dissipation rates (different rotational speeds of conventional stirring by impeller), and on different MgF_2 particle size distributions. The enhancement of the leaching rate due to ultrasound is found to occur in two steps: (1) MgF_2 particle fragmentation leading to high specific solid−liquid interfacial area and by increase in the surface diffusional rate of the reactive species; (2) enhancement in the convective diffusivity of the leach acid solvent through micropores of the MgF_2 agglomerate structure due to convective motion created by the cavitation phenomena (shock wave propagation, microjet formation) at the solid−liquid interface. Thus, the overall recovery has been increased by the application of ultrasound with several additional advantages such as low leach acid concentration and decrease in the leaching operation time. The energy dissipation rate with the use of ultrasound was very high, yet, at an equivalent energy dissipation rate in the form of conventional stirring, leaching rates or the final extent of the leaching could not be matched. This indicated that the scale (time and spatial) of energy dissipation has important effect on the overall leaching rate. Kinetics shows that the leaching operation can be explained as a classical shrinking core kinetics phenomenon with pore diffusion resistance as the rate-limiting step.

1. Introduction

Metal leaching operation is popular in the hydrometallurgical industry. Leaching, which is liberation of the metals from ores by chemical dissolution, forms the basis of most of the hydrometallurgical extraction processes. Leaching is an established and relatively successful method of metal extraction, especially when treating high grade ores. The main aim of leaching is to recover selectively the maximum amount of valuable metal. Uranium is the most precious metal obtained in the earth crust in a low parts per million level. Particularly in the lean grade uranium leaching process, conventional ore-dressing techniques have not been successful in the preconcentration of the uranium minerals.[1] However, it is usually possible to obtain acceptable recovery ratios. Recently, the use of ultrasonics through a process of cavitation in the form of shock waves and through microjet formation through a cavitating medium having elastic properties, such as water, gas, saturated water, and aqueous particle slurry suspensions, have shown to improve the rate of chemical reactions and has given better overall conversions.[2−5] Shock waves from cavitation in liquid−solid slurries produce high velocity intraparticle collisions. Ultrasound also improves the local transport in liquid systems by acoustic streaming. Acoustic waves are known to produce time-independent vortices in the pores of the suspended solids in aqueous solution as well as at solid−liquid interfaces.[6−11] Over the past few years, a large number of researchers working in material processing and metal extraction have developed an interest in the application of power ultrasound for industrial use.[12−14] Sonochemical extraction techniques together with classical methods gave a faster[15] and selective[16] extraction of metals. Orlov[17] and Chizhikov et al.[18] used ultrasound for Cu leaching from copper ores using sulfuric acid and reported that the time of leaching could be reduced by nearly 12 times by the action of ultrasound. Shukla et al.[19] reported the selective leaching of nickel over that of iron under the presence of ultrasound. Application of ultrasound in extractive metallurgy has been reviewed by Polyukhin.[20] The kinetics of the ultrasound assisted leaching of phosphate rock in HNO_3 is modeled by Tekin et al.,[21] and that in HCl, by Tekin.[22] Tarasova et al.[23] and Rao et al.[24] have used short ultrasonic pulses of higher intensities at the start of leaching for typical ores such as nickel laterites in Greece and ammonical leaching of copper oxide ore. The use of ultrasound in nickel extraction from lateritic nickel ore using a strain of *Aspergillus niger* was studied by Swamy et al.[25] It is generally understood that the process intensification can be expressed as follows: faster reactions, better conversions or higher recoveries, and fewer byproducts. Such improvements should, of course, be accompanied by simplification of the production line and lower production costs. Some of these targets can be achieved by the use of power ultrasound.

In the present work, leaching of uranium from tailings (MgF_2) has been studied with the optimization of the parameters in a conventional agitation method and under the influence of ultrasound. Improvement in the leaching rate is explained on the basis of the particle disintegration process and enhanced convective diffusivity of the leach acid during the ultrasonic treatment of leaching slurry. A kinetic model for the enhancement of leaching characteristics of uranium from MgF_2 has been proposed. On the basis of this model, a parameter (convective diffusivity constant) has been defined to quantify the improvement in the mass transfer rate. An attempt is made to match the energy dissipation rate through ultrasound and the mechanical agitation process and find the effect of the mode of energy dissipation (local energy dissipation pattern) on the leaching rate process.

* To whom correspondence should be addressed. E-mail: abp@udct.org. Tel.: +91-22-4145616. Fax: +91-22-4145614.

[†] Institute of Chemical Technology.

[‡] Bhabha Atomic Research Center (BARC).

10.1021/ie060599x CCC: $33.50
Published on Web 09/12/2006

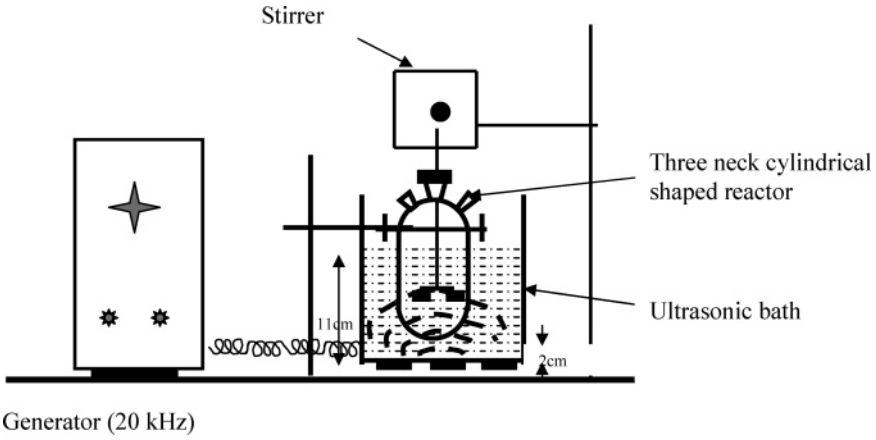

Figure 1. Experimental setup.

2. Experimental Work

The raw material used was MgF_2, a byproduct during the final processing of uranium ingot, where pure magnesium (Mg) is used as a reducing agent which reacts with the fluorine of UF_4 during the process, forming MgF_2, which contains a small amount of uranium: 2.89% in the particle size (−60 +200 mesh) ∼230 μm and 6.03% uranium in the particle size (+60 mesh) ∼420μm, obtained from the U.E.D., B.A.R.C., India. This crushed MgF_2 material used in the present investigation contains a small percentage of uranium. Experiments were performed in a 200 mL three neck cylindrical shaped round-bottom glass reactor (10 cm height and 5 cm internal diameter). The 20 kHz frequency irradiations (with a delivered power of 36 W) were used in an ultrasonic cleaning bath type system having dimensions of height, width, and breadth of 15 cm × 15 cm × 15 cm, respectively (Supersonics, Ultrasonic system, Mumbai). The distance between the cylindrical reactor bottom and the ultrasonic bath is maintained at 2 cm, and the liquid pool is maintained up to 11 cm in the ultrasonic bath, covering the entire acid slurry solution in the reactor that is exposed to the external ultrasonic bath side liquid medium. In the conventional stirring based leaching process, the agitator used was a 45° pitch 6 blade down pumping impeller (impeller diameter = 3.8 cm, $N_p \approx 2$) which have a good suspension characteristics for the solid particles. Impeller speed was varied using a variable speed drive motor with a display indicating impeller rotational speed (rpm). A schematic diagram of the experimental setup is shown in the Figure 1. The temperature was maintained at just above room temperature (30 °C) for all the experimental runs. Solid loading of 50% (50 g of MgF_2 in 100 mL of leach acid solution of different concentrations) weight by volume has been used. The leach acid used for this purpose was of different concentrations of HNO_3 namely 5, 7.5, and 10 vol % equivalent to 0.57, 0.88, and 1.19 N, respectively (HNO_3 was procured from S.D. Fine chemicals Ltd., analytical reagent). Distilled water has been used for all the experiments in the preparation of different concentrations of the leach acid solutions. Leach liquor solutions were analyzed for uranium content using an UV−vis spectrophotometer (chemito model-2500) at the absorbance wavelengths of 420 and 475 nm depending on the strength of the uranium content in the complex formed with the solution of ethanolic ammonium thio-cyanate and stannous chloride (9:1) with aluminum nitrate as the salting agent (Thomas Baker., analytical reagent). The particle size distribution of the MgF_2 has been measured with an LS-230 Coulter particle size analyzer (laser diffraction method). All the experiments were carried out in duplicate and sometimes repeated again, and the mean values have been reported. The maximum standard deviation observed between the reported experiments never exceeded beyond ±4%.

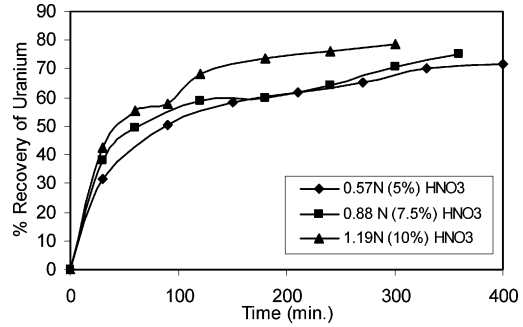

Figure 2. Effect of the leach acid concentration on uranium recovery from a particle size range of (−60 +200) ∼230 μm by stirring (silent conditions).

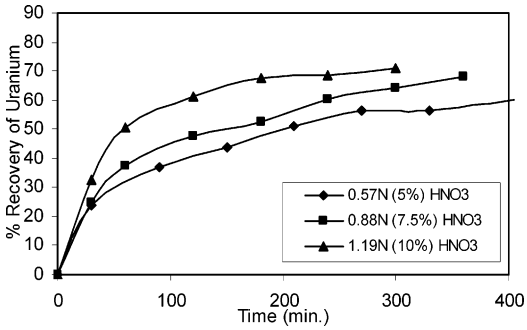

Figure 3. Effect of the leach acid concentration on uranium recovery from a particle size range of (+60) ∼420 μm by stirring (silent conditions).

3. Results and Discussion

3.1. Effect of Leach Acid Concentration. Experiments were carried out using three different leach acid concentrations i.e., 5, 7.5, and 10% nitric acid (HNO_3) equivalent to 0.57, 0.88, and 1.19 N, respectively. As can be seen from Figures 2 and 3, the results for both the particle size ranges with leaching under only stirring (silent) conditions are showing significant differences in the leaching rate with an increase in the leach acid concentration. For smaller particles (230 μm), the improvement in the overall recovery of the uranium is 9.14%, and for the bigger particle size (420 μm), the improvement in the overall recovery is 14.2% as we increase the leach acid concentration from 0.57 N (5% HNO_3) to 1.19 N (10% HNO_3) under the stirring speed of 1000 rpm, over the same period of leaching operation (∼6 h). The possible reason for the enhancement in the leaching rate with an increase in the leach acid concentration

Table 1. Particle Size Distributions of Leached Particles of MgF_2 under Different Operating Conditions

particle size	particle size distribution[a] ($10^6 \times$ m)	σ_{sd}/d_p(avg)
Particle Size Range (−60 +200) ∼230 μm		
5.0% HNO_3 (1000 rpm ∼ 8.85 kW/m^3)	223.6	0.426
7.5% HNO_3 (1000 rpm ∼ 8.91 kW/m^3)	214.8	0.465
10% HNO_3 (1000 rpm ∼ 8.97 kW/m^3)	183.3	0.544
5.0% HNO_3 (US +1000 rpm ∼ 29.77 kW/m^3)	154.1	0.541
7.5% HNO_3 (US +1000 rpm ∼ 29.83 kW/m^3)	154.9	0.673
10% HNO_3 (US +1000 rpm ∼ 29.89 kW/m^3)	152.6	0.635
5% HNO_3 (600 rpm ∼ 1.91 kW/m^3)	221.2	0.489
5% HNO_3 (1000 rpm ∼ 8.85 kW/m^3)	223.6	0.426
5% HNO_3 (1500 rpm ∼ 29.86 kW/m^3)	227.3	0.424
5% HNO_3 (1800 rpm ∼ 51.58 kW/m^3)	218.3	0.471
Particle Size Range (+60) ∼ 420 μm		
5.0% HNO_3 (1000 rpm ∼ 8.85 kW/m^3)	399.4	0.489
7.5% HNO_3 (1000 rpm ∼ 8.91 kW/m^3)	406.5	0.625
10% HNO_3 (1000 rpm ∼ 8.97 kW/m^3)	357.8	0.483
5.0% HNO_3 (US +1000 rpm ∼ 29.77 kW/m^3)	335.6	0.543
7.5% HNO_3 (US +1000 rpm ∼ 29.83 kW/m^3)	346.5	0.954
10% HNO_3 (US +1000 rpm ∼ 29.89 kW/m^3)	195.7	0.531
5% HNO_3 (600 rpm ∼ 1.91 kW/m^3)	410.6	0.478
5% HNO_3 (1000 rpm ∼ 8.85 kW/m^3)	399.4	0.489
5% HNO_3 (1500 rpm ∼ 29.86 kW/m^3)	372.4	0.498
5% HNO_3 (1800 rpm ∼ 51.58 kW/m^3)	382.6	0.490

[a] Measured using a Coulter LS 230 particle size analyzer.

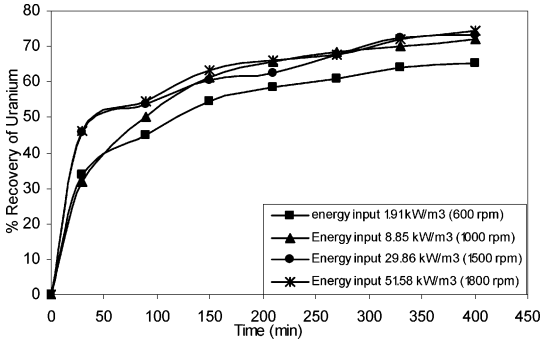

Figure 4. Effect of the energy input of stirring on the leaching rate for a particle size of (−60 +200) ∼230 μm.

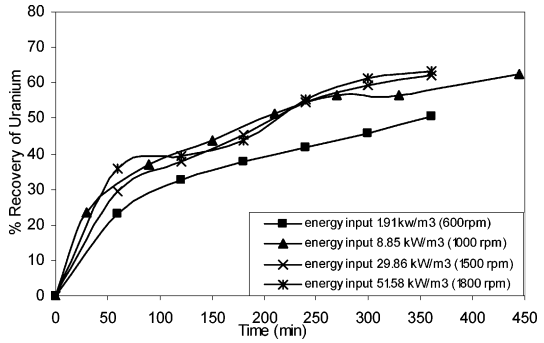

Figure 5. Effect of the energy input of stirring on the leaching rate for a particle size of (+60) ∼420 μm.

is explained on the basis of the observed particle size disintegration process shown in Table 1. Leaching beyond 600 rpm is an internal (micropore) diffusion mass transfer controlled reaction, and under low leach acid concentration, the leaching acid cannot effectively breakdown the magnesium fluoride (MgF_2) structure restricting the penetration of the leaching solution to the center (inside the MgF_2 matrix) to extract the uranium. At higher leach acid concentration (i.e., 1.19 N leach acid), the MgF_2 particles are disintegrating (disintegrated) faster to a smaller particle size, exposing a larger surface area. Also, the controlling mechanism for the leaching operation is shifting from a pore diffusion controlled mechanism to a surface (film) diffusion mechanism as the leach acid concentration is increased from 0.57 to 1.19 N. The particle size distribution of the MgF_2 before and after the leaching operation clearly indicates that the enhancement in the leaching rate is due to the breakdown of the MgF_2 agglomerate (matrix structure). It is observed from Table 1 that the mean value of the leached out particles size is shifting toward the smaller mean particle size of 223 to 183 μm from a starting mean particle size of 230 μm and to 406 to 357 μm from a starting mean particle size of 420 μm, as the concentration of the leach acid is increased from 0.57 to 1.19 N over the same stirring treatment period. The values of the average particle size and the parameter ($\sigma_{s,d}/d_p$(avg)) indicating the spread of the distribution of the particles are also mentioned in Table 1. It can be observed that the higher value of parameter ($\sigma_{s,d}/d_p$(avg)) indicating the spread of the distribution of the leached out particles is greater under ultrasound irradiation than under stirring conditions.

3.2. Effect of Energy Input by Conventional Stirring Process. Experiments have been performed under different energy input levels using the conventional stirring process. Rotational speeds of the impeller maintained were at 600, 1000, 1500, and 1800 rpm which corresponded to 1.91, 8.85, 29.86, and 51.58 kW/m^3 of energy dissipation rates (Appendix A). Both particle sizes (the smaller (−60 +200) ∼230 μm and higher (+60) ∼420 μm diameter particle sizes) have been used over the above stated energy dissipation rates. The effect of the energy dissipation on the leaching rate of uranium for both the particle size ranges through the conventional stirring process have been shown in Figures 4 and 5 for smaller and larger particle sizes, respectively. It is observed from Figure 4 that the increase in the energy input by conventional stirring does not show much improvement on the leaching rate for a small particle size range (∼230 μm) beyond an energy input rate of 1.91 kW/m^3 (corresponding to 600 rpm). The possible reason for this may be that beyond the energy dissipation rate of 1.91 kW/m^3 (600 rpm), the external mass transfer resistance has been completely eliminated and the internal (pore diffusion) mass transfer resistance becomes a rate controlling step which is unaffected by external agitation. With an increase in the energy input rate from 1.91 to 8.85 kW/m^3 (600 to 1000 rpm) using stirring, the enhancement in the overall recovery of uranium

after 6 h of stirring is only 10.1%. Further increase in the energy input rate from 8.85 to 51.58 kW/m^3 (1000 to 1800 rpm) has not shown substantial improvement in the leaching rate, i.e., only by a further 3.4%.

The effect of energy input by stirring on the leaching rate for a bigger particle size (~420 μm) is shown in Figure 5. It can be seen from Figure 5 that, as the energy input rate is increased from 1.91 to 8.85 kW/m^3 (600 to 1000 rpm) by stirring, the enhancement in the overall recovery of uranium after 6 h of stirring operation is by 15.3% which is marginally higher than that observed for the lower particle size (~230 μm). Further increase in the energy input rate from 8.85 to 51.58 kW/m^3 (1000 to 1800 rpm) showed again an increase in the uranium recovery, i.e., by 8.8% versus only 3.4% observed for smaller particles. This could be due to the fact that for the larger size particles with reduced solid surface area per unit volume, higher energies are required to keep the particles in the suspension as well as to distribute them uniformly in order to overcome the external mass transfer resistances including the available exposed surface area for the reaction.

3.3. Effect of Ultrasound on the Leaching Rate and on the Leaching Efficiency. Results have clearly shown greater improvement in the leaching rate under ultrasound initiated cavitation conditions than under stirring conditions at equivalent power input levels, and the enhancement in the leaching rate with the use of ultrasound is much higher at lower leach acid concentration than at high leach acid concentration. The observed enhancement in the leaching rate at low leach acid concentration in the presence of ultrasound can be again explained on the basis of the particle size disintegration process shown in Table 1. As it was explained in section 3.1, at low leach acid concentration, the leaching is a pore diffusion mass transfer controlled operation as this low acid strength cannot effectively breakdown the magnesium fluoride (MgF_2) structure. The physical effects of the cavitation, such as the shock waves and microjet formation, are enhancing the intraparticle leach acid convective diffusion and hence the internal (within the pore) mass transfer rate. Thus, the leaching solvent is able to penetrate into the solid matrix and undergo the reaction with the solute. At higher leach acid concentration (i.e., 1.19 N leach acid), the MgF_2 particles are broken down (disintegrated) into a smaller particle size. The particle size distribution of the MgF_2 before and after the leaching operation under ultrasound cavitation clearly indicates that the enhancement in the liquid penetration is due to the breakdown of the MgF_2 agglomerate (matrix structure). Ultrasonic irradiation further reduces the particles to a smaller size (~160 and ~360 μm mean sizes starting from initial particle sizes of ~230 and ~420 μm, respectively). It can be observed from Table 1 that the average value of leached out particle size is decreased to ~152 μm from a starting mean particle size of 230 μm and to 335 to 195 μm from a starting mean particle size of 420 μm, as the concentration of the leach acid is increased from 0.57 to 1.19 N over the same treatment period in the presence of ultrasound.

One more interesting feature has been observed from the leaching rates of the uranium. There are two distinct regimes of leaching: initially, the leaching rate is high up to a certain period (around 40−45 min) of the leaching operation and then gradually decreases showing a very little or no further increase in the uranium concentration in the leached liquid for some period, and then, the leaching rate again increases although it is much lower than the initial leaching rate. Thus, the metal removal process is expected to have two steps, with different leaching rates: (1) an initial higher rate of leaching, in which only for a smaller time period of leaching during which only surface metal residing on the MgF_2 matrix is removed; (2) a leaching rate for an extended time period of leaching during which both surface and metal present interior to the MgF_2 matrix is removed. It is obvious that the metal leaching rate for step 1 is higher than for step 2. The leaching rate enhancement for step 1 is higher due to ultrasound irradiation than that for step 2; this is due to the fact that most of ultrasound cavitational events are bound to occur on the surface of MgF_2 particles. The leaching rate enhancement for step 1 due to ultrasound irradiation is higher for smaller particles (−60 +200) ~230 μm than bigger particles (+60) ~420 μm. This can be seen from Figures 6 and 7. A similar phenomenon was observed by Moholkar and Warmoeskerken[26] during textile treatment by ultrasound; they attributed these two distinct rates to inter- and intra-yarn resistances of the textile material. The possible reason for these two distinct rates of uranium leaching is explained as follows: in the initial phase of the leaching, the uranium which is there (possibly in the adsorbed state) on the surface of the MgF_2 matrix has been leaching out

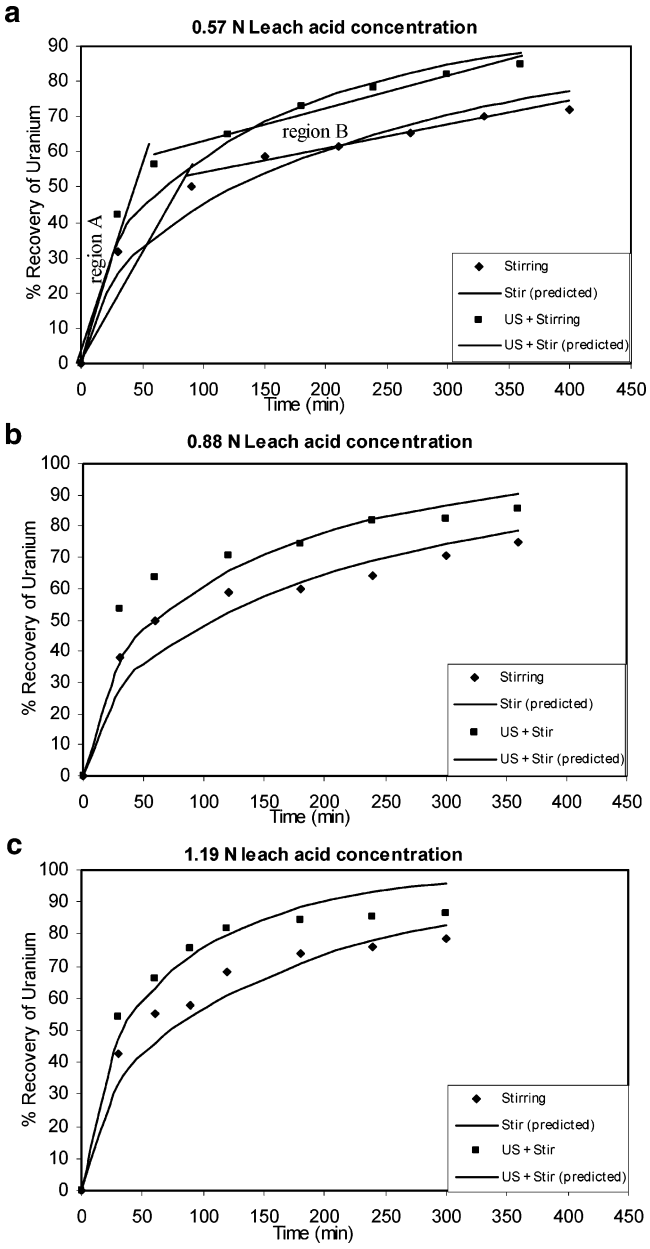

Figure 6. Effect of ultrasound and stirring on the leaching rate of uranium at different leach acid concentration solutions in a particle size range of (−60 +200) ~230 μm.

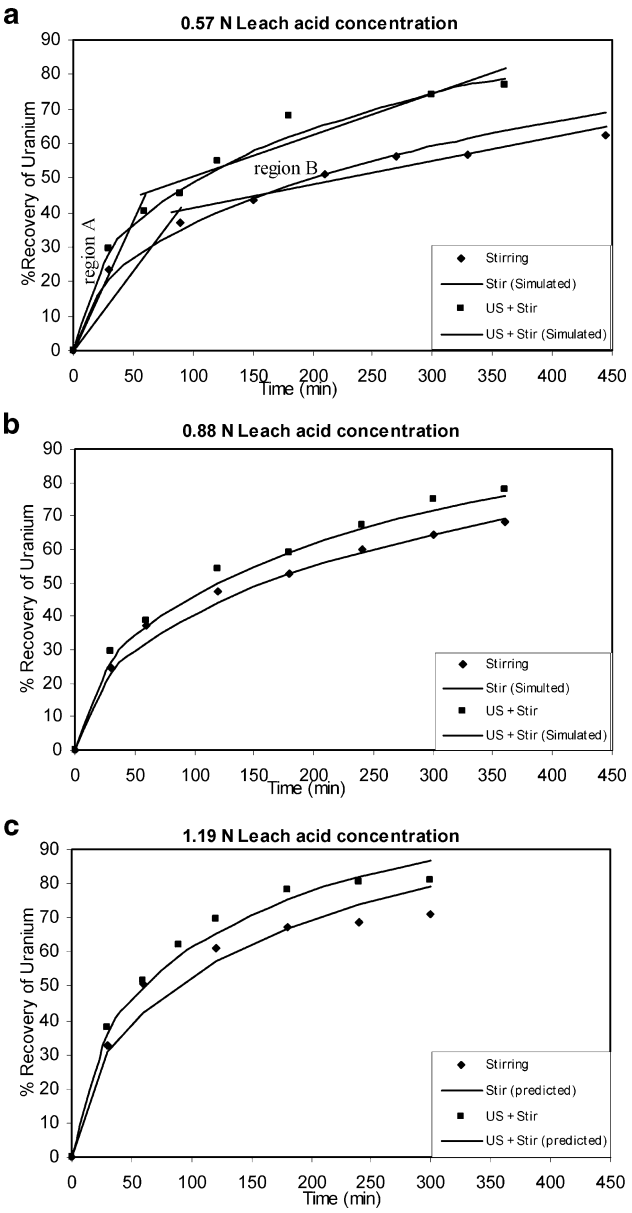

Figure 7. Effect of ultrasound and stirring on the leaching rate of uranium at different leach acid concentration solutions in a particle size range of (+60) ~420 μm.

(film diffusion controlling step), and then, during the second phase of the leaching, the uranium which is inside the solid particles (pores) starts reacting with the HNO_3. Some specific time is required for the leach acid solution to reach the particle interior through the convective diffusion process after which the leaching rate increases again (MgF_2 pore diffusional controlling step). At a particular concentration of the leach acid, the shift between the first regime to the second regime is occurring much earlier under ultrasound conditions than under stirring conditions, indicating that the formation of shock waves upon the cavity collapse and asymmetric collapse of the cavity in the surroundings of the solid particle results into microjets that are causing early penetration of the leach acid and its subsequent reaction with the metal which is residing within the particle, showing earlier transition to the second regime.

From Figure 6, a maximum recovery of 78.4% of uranium for the particle size range (−60 +200) ~230 μm is achieved with a (10%) 1.19 N leach acid concentration, whereas only 71% recovery has been obtained when the acid concentration is reduced to 0.57 N within 6 h of the leaching operation under stirring conditions. 84.8% overall recovery of uranium metal has been achieved with a 0.57 N leaching solvent acid concentration over the same period of 6 h under ultrasound irradiation, i.e., nearly a 20% increase in the overall recovery rate has been acheived. Thus, the advantage of the low acid concentration (leach acid strength) with the energy dissipation in the form ultrasonic irradiation power (increasing the power dissipation rate by the conventional stirring process does not show this enhancement). Calculations of the energy dissipation by stirring and ultrasound irradiation processes have been given in Appendices A and B. Similarly, for the particle size of (+60) ~420μm, it can be seen from Figure 7 that the overall recovery has been increased to 77% from 62.3% (nearly 24% increase) at 5% (0.57 N) leach acid concentration by the application of ultrasound.

4. Modeling of the Metal Leaching Kinetics

4.1. Classical Shrinking Core Model. The reaction mechanism assumed in this study is a simplification of the reaction zone model proposed by Braun et al.[27] This model proposes a mixed leaching kinetics involving a surface reaction and pore diffusion through a reacted porous zone surrounding the region of unreacted core. Assuming the surface reactions were fast enough, uranium leaching from a spherical ore particle would become pore diffusion controlled. The kinetics can be described by the equations as follows,[28]

$$\frac{t}{\tau} = 1 - 3(1 - L)^{2/3} + 2(1 - L) \qquad (1)$$

where τ = total leaching time (complete conversion) (min), L = fraction of uranium leached, r_c = the radius of the unreacted core at time t, and R = the radius of the ore particle.

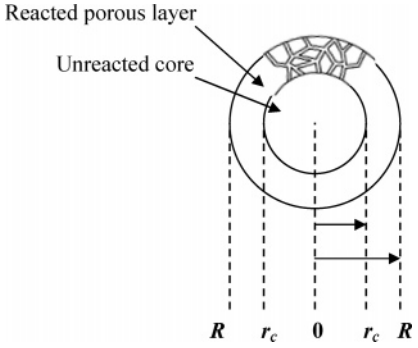

The total conversion time τ is obtained by plotting $(1 - 3(1 - L)^{2/3} + 2(1 - L))$ versus t and by determining the slope of the line. Also, 70% of the uranium recovery time ($t_{70\%}$) is readily calculated from the above eq 1, by substituting the $L(t) = 0.7$ giving $\Rightarrow t_{70\%} = 0.25 \times \tau$. The values of the total leaching (recovery) time (τ), 70% of the uranium leaching (recovery) time, and the model predicted leaching times are given in Table 2.

The leaching rate data of the different experiments under different conditions have been fitted to the above derived shrinking core model, and the results of the correlation coefficients (R) and the predicted total time for the complete recovery is tabulated in Table 2. The predicted time for the complete recovery is more for a bigger particle size than the smaller size particles. The validity of the model is expressed by comparing the experimental data and the model-predicted values using the correlation coefficients (R). A relatively high value of the correlation coefficient (near to unity) indicates that the model successfully describes the kinetics of the uranium leaching from MgF_2.

Table 2. Values of the Total Time of Recovery, 70% Metal Leaching Time, and Correlation Coefficient

particle size	predicted time of overall metal leaching (τ) (min)	predicted 70% metal leaching time ($t_{70\%}$) (min)	experimental 70% metal leaching time ($t_{70\%}$) (min)	R
Particle Size Range (−60 +200) ~230 μm				
5.0% HNO_3 (1000 rpm ~ 8.85 kW/m^3)	1250	319	326	0.8645
7.5% HNO_3 (1000 rpm ~ 8.91 kW/m^3)	1111	284	290	0.8816
10% HNO_3 (1000 rpm ~ 8.97 kW/m^3)	714	182	140	0.8479
5.0% HNO_3 (US +1000 rpm ~ 29.77 kW/m^3)	714	182	160	0.9364
7.5% HNO_3 (US +1000 rpm ~ 29.83 kW/m^3)	667	170	116	0.7917
10% HNO_3 (US +1000 rpm ~ 29.89 kW/m^3)	476	121	75	0.6152
5% HNO_3 (600 rpm ~ 1.91 kW/m^3)	1667	426		0.8618
5% HNO_3 (1000 rpm ~ 8.85 kW/m^3)	1250	319	326	0.8645
5% HNO_3 (1500 rpm ~ 29.86 kW/m^3)	1250	319	300	0.8159
5% HNO_3 (1800 rpm ~ 51.58 kW/m^3)	1111	283	301	0.7856
Particle Size Range (+60) ~420 μm				
5.0% HNO_3 (1000 rpm ~ 8.85 kW/m^3)	2000	511		0.9516
7.5% HNO_3 (1000 rpm ~ 8.91 kW/m^3)	1429	365	370	0.9878
10% HNO_3 (1000 rpm ~ 8.97 kW/m^3)	909	232	270	0.8517
5.0% HNO_3 (US +1000 rpm ~ 29.77 kW/m^3)	1000	255	220	0.9624
7.5% HNO_3 (US +1000 rpm ~ 29.83 kW/m^3)	1000	255	261	0.994
10% HNO_3 (US +1000 rpm ~ 29.89 kW/m^3)	625	159	125	0.8869
5% HNO_3 (600 rpm ~ 1.91 kW/m^3)	3333	851		0.9959
5% HNO_3 (1000 rpm ~ 8.85 kW/m^3)	2000	511		0.9918
5% HNO_3 (1500 rpm ~ 29.86 kW/m^3)	2000	511		0.9929
5% HNO_3 (1800 rpm ~ 51.58 kW/m^3)	1667	426		0.9699

4.2. Leaching Rate Enhancement (Convective Transport of HNO_3) Due to Ultrasound. The rate of leach acid diffusion through the micropores of the MgF_2 particles is the rate controlling step especially in the later stages of the operation, and this is probably true for the system under consideration (uranium leaching with HNO_3 from MgF_2). For isothermal diffusion in a spherical particle, the flux of the component "A" (HNO_3) is important in the transfer process.

The component A throughout the MgF_2 agglomerate particle is given by[29,30]

$$L(t) = \frac{L_d}{L_o} = 1 - \frac{6}{\pi^2}\sum_{n=1}^{\infty}\exp\left(-\frac{n^2\pi^2 D}{r_o^{\,2}}t\right) \qquad (2)$$

Where, L_d is the amount of solute leached at time t (mg/g), L_o is the total amount of leach solute (mg/g), n is the integer that defines the infinite series solution, D is the solvent diffusion coefficient (m^2/s), t is the time (s), r_o is the particle (MgF_2 agglomerate) radius (m), and (L_d/L_o) is the leached fraction $L(t)$.

For $L(t) > 0.8$, the terms higher than first order in eq 2 can be neglected. For more convenient and practical use, Vermeulen's approximation[31] which fits the whole range $0 \le L(t) \le 1$ can be used and is given by

$$L(t) = \left[1 - \exp\left(-\frac{Dt\pi^2}{r_o^{\,2}}\right)\right]^{1/2} \qquad (3)$$

The (relative) leaching rate thus is proportional to the solvent diffusion coefficient in the MgF_2 and inversely proportional to the square of the MgF_2 particle radius.

Rearranging eq 3 to the form

$$-\ln[1 - (L(t))^2] = \left(\frac{D\pi^2}{r_o^{\,2}}\right)\cdot t \qquad (4)$$

The convective diffusivity coefficient (D/r_o^2)is obtained by plotting the graph between $-\ln[1 - (L(t))^2]$ versus t and by determining the slope of the line. The values of the convective diffusivity coefficient (D) are obtained by multiplying the average particle size of the MgF_2. The validity of the leaching acid (HNO_3) transport model is expressed by comparing the experimental data and the model simulated curves given in Figures 6 and 7, and relatively high values of the correlation coefficient (near to unity) indicate that the model successfully describes the transport of the leaching acid (HNO_3) through the pores of the particle. The 70% metal leaching time predicted by the model and the experimentally observed 70% metal leaching time are of the order of minutes, as it can be seen from Table 2. The ($t_{70\%}$) time of the metal recovery has reduced from 326 to 160 min at 5% (0.57 N) leach acid concentration by the application of the ultrasound compared to only stirring conditions for this particle size (~230 μm). The 70% metal leaching time for all the leach acid concentrations can be seen from Table 2 for both the particle size ranges studied in this work. The discrepancy in the predicted 70% metal recovery time from the experimental time of metal recovery ($t_{70\%}$) in Table 2 and the low values of the correlation coefficients (R) in the Table 3 are due to the assumption of constant diffusion coefficient made in the model. In actual practice, two diffusional resistances, film diffusion (step 1) and pore diffusion (step 2), offering the two different diffusional coefficients have been observed (region A and B having different slopes) in Figure 6a. The values of the diffusional coefficient are higher for step 1 than step 2. We have approximated the leaching curves in terms of two different mass transfer rates (slopes) for these two steps (region A and region B) as straight lines shown in Figures 6a and 7a for both the smaller and the larger particles under 0.57 N leach acid concentration. The slope values of the straight lines are given in Table 4, these values are clearly indicating the difference in the mass transfer rates for the two regions. It can be observed, from Table 4, that the values of external and internal mass transfer (leaching) rates for the smaller particles (~230 μm) are increased by 70% and 38% respectively by the application of ultrasound, whereas for the larger particles (~420 μm) the improvement in these rates are 63% and 71%, respectively. This indicates that the ultrasound irradiation is much more effective on larger particles in order to overcome the internal masstransfer resistance (pore resistance). As a result of this difference in the mass transfer rates, the discrepancy has been observed between the predicted and experimental values of ($t_{70\%}$) for smaller particles (~230 μm). Relatively good prediction for larger particles (~420 μm) indicates that the leaching operation is mostly pore diffusion controlled in the case of the larger

Table 3. Values of the Convective Diffusion Coefficient and Correlation Coefficient

particle size	(D/r^2) $(10^6 \times s^{-1})$	convective diffusivity coefficient (D) ($10^{13} \times m^2/s$)	R
Particle Size Range (−60 +200) ∼230 μm			
5.0% HNO_3 (1000 rpm ∼ 8.85 kW/m^3)	3.719	1.91	0.9211
7.5% HNO_3 (1000 rpm ∼ 8.91 kW/m^3)	3.888	1.92	0.9059
10% HNO_3 (1000 rpm ∼ 8.97 kW/m^3)	6.254	2.67	0.8700
5.0% HNO_3 (US +1000 rpm ∼ 29.77 kW/m^3)	6.424	2.37	0.9597
7.5% HNO_3 (US +1000 rpm ∼ 29.83 kW/m^3)	6.931	2.57	0.8461
10% HNO_3 (US +1000 rpm ∼ 29.89 kW/m^3)	9.804	3.59	0.6898
5% HNO_3 (600 rpm ∼ 1.91 kW/m^3)	2.705	1.38	0.8615
5% HNO_3 (1000 rpm ∼ 8.85 kW/m^3)	3.719	1.91	0.8726
5% HNO_3 (1500 rpm ∼ 29.86 kW/m^3)	3.719	1.94	0.8292
5% HNO_3 (1800 rpm ∼ 51.58 kW/m^3)	3.888	1.95	0.8026
Particle size Range (+60)∼ 420 μm			
5.0% HNO_3 (1000 rpm ∼ 8.85 kW/m^3)	2.028	2.01	0.9492
7.5% HNO_3 (1000 rpm ∼ 8.91 kW/m^3)	3.042	3.08	0.9875
10% HNO_3 (1000 rpm ∼ 8.97 kW/m^3)	4.733	4.47	0.8578
5.0% HNO_3 (US +1000 rpm ∼ 29.77 kW/m^3)	4.564	3.65	0.9686
7.5% HNO_3 (US +1000 rpm ∼ 29.83 kW/m^3)	4.395	3.65	0.9936
10% HNO_3 (US +1000 rpm ∼ 29.89 kW/m^3)	7.269	3.43	0.9061
5% HNO_3 (600 rpm ∼ 1.91 kW/m^3)	1.352	1.39	0.9942
5% HNO_3 (1000 rpm ∼ 8.85 kW/m^3)	2.028	2.01	0.9492
5% HNO_3 (1500 rpm ∼ 29.86 kW/m^3)	2.367	2.15	0.9935
5% HNO_3 (1800 rpm ∼ 51.58 kW/m^3)	2.536	2.38	0.9696

Table 4. Values of Slopes of the Approximated Straight Lines

	stirring		ultrasound	
	step 1	step 2	step 1	step 2
particle size range (−60 +200) ∼230 μm	0.609	0.068	1.035	0.094
particle size range (+60) ∼420 μm	0.448	0.070	0.731	0.120

particles. Close observation also indicates that, at higher leach acid concentrations, the difference in the predicted and experimental times is also large. This can be attributed to the change in the MgF_2 matrix structure due to acid attack, altering the diffusion coefficients in the middle of the leaching operation.

5. Quantification of Mass Transfer Enhancement: Concept of the Convective Diffusive Coefficient

It was shown[26,32] that (high energy) transient bubble motion near the solid surface is responsible for the creation of strong convection in the close vicinity of the solid surface, which enhances the mass transfer rate. However, the bubble motion near a solid boundary is a multifaceted phenomenon. The micromechanism of this process is not clear. It is not known exactly by which mechanism, viz., shock wave, high velocity microjet, or oscillatory spherical velocity field generated due to radial bubble motion or by combination of all the three possibilities, the convection responsible for the mass transfer enhancement is caused. Most of the bubble dynamics equations available so far[34−36] use a single bubble oscillating in an infinite medium. However, in practical situations, such as the current study, the net physical/chemical effect is a result of multibubble phenomena. A comprehensive model that describes dynamics of thousands of bubbles, with strong interaction between them, has not yet been developed. We, therefore, adopt a semiempirical method to estimate the mass transfer enhancement by convective diffusive coefficient (D); this is representative of the mass transfer enhancement due to ultrasonic irradiation. This convective diffusion coefficient in the present study is determined to be in the range $10^{-12}-10^{-13}$ m^2/s, which is in the accepted range of results published in the literature.[26] Under these operating conditions, the diffusivity coefficient of leach acid through the pores is calculated to be in the range of $10^{-12}-10^{-13}$ m^2/s and is given for all operating conditions in Table 3.

From Table 3, it can be seen that at 5% (0.57 N) leach acid concentration the value of the convective diffusivity coefficient of the leach acid solution for the particle size of (−60 +200) ∼230 μm is enhanced only by 2.1% (1.91−1.95) and for the particle size of (+60) ∼420 μm it is enhanced by 18.4% (2.01 to 2.38) by increasing the energy dissipation rate from 8.85 to 51.58 kW/m^3 through stirring. At the same time, the enhancement in the diffusivity coefficient for the particle size of (−60 +200) ∼230 μm is 24.1% (1.91 to 2.37) and for the particle size of (+60) ∼420 μm it is 81.6% (2.01 to 3.65) by increasing the power dissipation rate from 8.85 to 29.77 kW/m^3 in the form of ultrasonic irradiation. The enhancement in the convective diffusivity coefficient by the application of ultrasonic irradiation can be attributed to asymmetric cavity collapse leading to microjets targeted to the solid surface, high pressure shock waves generated by the cavity collapse, and acoustic vortex microstreaming produced within the pores as well as at the solid−liquid interface. During the bubble collapse, however, material is torn off the particles which results in a size reduction of the MgF_2 particles. When bubbles are produced close to the solid boundary, the localized hot spots generate high temperatures and pressures at the surface of the MgF_2 particle surface increasing the solubility of the solute. Thus, the leaching rate has been found to increase with ultrasonic irradiation.

6. Measurement of the Rate of Change of the Surface Area of MgF_2 Particles

Most of the effects of ultrasound in heterogeneous reactions have been attributed to acoustic cavitation. On collapse, the contents of the bubble are heated to very high temperatures and are capable of producing shock waves and high velocity liquid microjets which, on interaction with the solid surface, can lead to particle fragmentation. Other possible mechanisms of solid fragmentations are the results of collision associated with the rapidly altering pressures in the liquid medium which may cause particles to reach very high accelerations. With such high acceleration, a particle can collide with an object in the reactor such as with another particle, resulting in fragmentation.

To show the surface area change due to these effects, we have considered the overall surface area change, and for this purpose, we have the equation for surface area change for a first-order heterogeneous reaction

$$-\mathrm{d}c/\mathrm{d}t = kSc \tag{5}$$

and

$$\mathrm{d}S/\mathrm{d}t = Sa_{\mathrm{av}} \tag{6}$$

Where, "c" is the concentration of the uranium component, "k" is the reaction rate constant, "S" is the solid surface area, and "a_{av}" is the specific surface area change rate which refers to the unit surface area of the solid. Under isothermal conditions, k is constant and then the solution for a_{av} is

$$a_{\mathrm{av}} = \frac{c\,\mathrm{d}^2c/\mathrm{d}t^2 - (\mathrm{d}c/\mathrm{d}t)^2}{c\,\mathrm{d}c/\mathrm{d}t} \tag{7}$$

The solid surface area at time t from eqs 5 and 6 is expressed as

$$\frac{S(t)}{S_0} = \frac{c_0\,\mathrm{d}c/\mathrm{d}t}{\mathrm{d}c/\mathrm{d}t\downarrow_{t=0}C} \tag{8}$$

S_0 is the initial solid surface area, and c_0 is the initial concentration of the uranium component. It is shown that the rate of change of the specific surface area as well as the total solid surface area can be described in terms of the change in the concentration of the uranium component. From eq 6, the specific surface area change rate (a_{av}) can be determined by plotting the changes of surface area vs time, i.e., $\ln(S_o/S_t)$ vs t. The slope of this curve gives the rate of change of the specific surface area; a_{av}. We can consider the detailed change of the surface area. The surface area change is due to particle fragmentation with ultrasound irradiation, due to the strength of the leach acid, and shrinking due to chemical reaction.

6.1. Particle Fragmentation. To examine the effect of the particle size reduction process in the form of increase in the surface area on the leaching rate enhancement, a separate set of experiments have been conducted under silent and ultrasound irradiation conditions on MgF_2 particles in water and 10% HNO_3 solution used as a leach solution. The MgF_2 particle size distribution under different operating conditions has been measured; the particle size distribution at varying time intervals (initial size distribution, 30, 90, 150, 210, 270, and 360 min) of operation have been measured by taking a small sample of 2 g. The surface area change is due to particle fragmentation with ultrasound irradiation, the strength of the leach acid, and shrinking due to chemical reaction. The particle disintegration process mechanism has been shown schematically in Figure 8. The variation in the mean particle size with respect to the time of operation is shown in Figure 9. As it is clear from Figure 9 with water as a leach solvent under stirring conditions (case 1), no considerable breakage (disintegration) of particles has been observed and the average particle size of MgF_2 particles (420 μm) remains at 415 μm. But with water as a leach solvent under ultrasound irradiation (case 2), the average size of the MgF_2 particles has been decreased from 420 to 350 μm. With 10% HNO_3 as a leach acid under stirring conditions (case 3), the average particle size of MgF_2 particles has been decreased to 357 μm, and with 10% HNO_3 leach acid solution under ultrasound irradiation conditions (case 4), the average particle size decreased to 195 μm over 6 h of operation. The corresponding changes in the specific surface area for all the four cases have been given in Table 5.

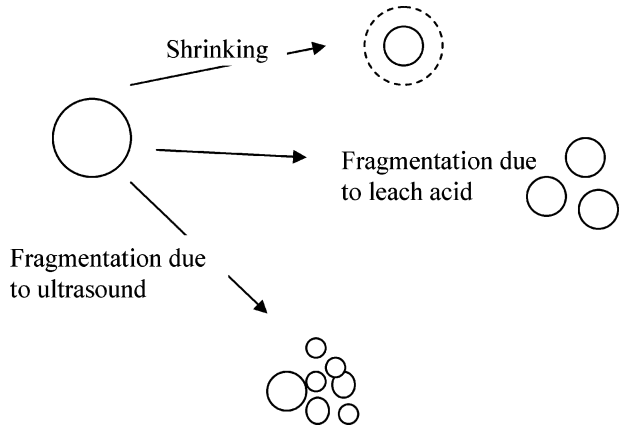

Figure 8. Mechanism of change of MgF_2 solid surface area.

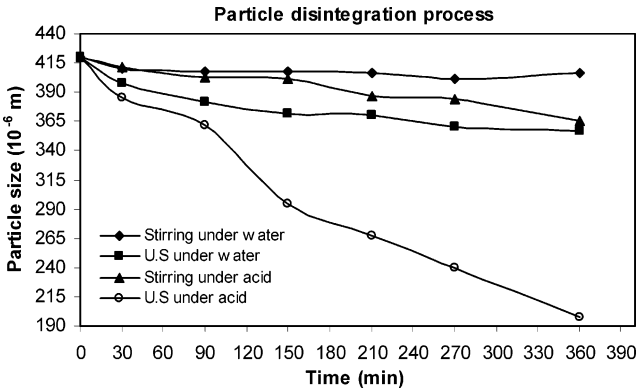

Figure 9. Particle disintegration process.

Table 5. Specific Surface Area Change with Respect to Time

S. no.	time interval (min)	case 1[a]	case 2[a]	case 3[a]	case 4[a]
1	initial	357.5	357.5	357.5	357.5
2	30	413.7	439.3	397.4	540.2
3	90	454.3	455.3	410.8	663.9
4	150	401.5	510.3	406.8	677.1
5	210	381.4	519.5	531.3	703.9
6	270	378.6	528.5	525.9	710.3
7	360	453.6	557.3	540.5	1216

[a] (m^2/m^3).

The change of surface area in heterogeneous reactions with ultrasound irradiation is reported by several authors.[36,37] The surface area changes as a result of cavitation by interparticle collision, particle fragmentation, chemical reaction, etc. which are coupled and very difficult to distinguish. The purpose of this session is to confirm that the improvement in the leaching rate under ultrasound irradiation is not only due to an increase in the surface area of the solid particle but also due to enhancement in the convective diffusivity.

As we have explained earlier, as the particle size decreases due to chemical reaction, the surface area should decrease but the experimental results (Table 5) show a reverse trend. The reason for increase in the surface area is due to particle size breakage (fragmentation) due to the strength of the leach acid, i.e., the rate of decrease of the particle size due to chemical reaction is less (as the uranium percentage is only ~6.03% in the MgF_2 particle) when compared to the rate of breakage (fragmentation) of particles due to the strength of the leach acid. Figure 9 and Table 5 clearly showing the rate of decrease of particle size due to fragmentation and the increase of surface area is enhanced due to ultrasound irradiation along with an increase in the strength of the leach acid concentration. The particle size and surface area distribution at each time interval

depends on the kinetics of breakage and leaching kinetics. The bigger particle disintegration rate is more due to ultrasound fragmentation than by the strength of the leach acid.

The mass transfer (leaching) rate is directly proportional to the specific surface area (a_{av}) when it is controlled by a film diffusion process. In this leaching process, the leaching experiments conducted with the average particle size of (+60) ~420 μm. The increase in the specific surface area (a_{av}) under the ultrasound irradiation compared to the increase in specific surface area (a_{av}) under stirring conditions over 5 h of leaching operation was 35% (from Table 5). The observed increase in the leaching rate under these two conditions is only 14% (from Figure 9c), indicating that the enhancement in the leaching rate is not directly proportional to the external average specific surface area (a_{av}).

The mass transfer process in this case is not the external film diffusion controlled process but is also affected by the intraparticle leach acid diffusivity. This also collaborates the earlier energy effect on stirring, which does not show a significant increase in the leaching rate with an increase in the energy dissipation. Ultrasonic irradiation is known to affect inter- and intra-particle diffusion phenomena and hence shows a significantly higher energy effect.

7. Conclusion

In this work, we have explored the effects of ultrasound on leaching of uranium from MgF_2 slag material. Improvement of the metal leaching from MgF_2 particles by ultrasound stems from enhancement of the surface diffusivity coefficient and as well as the particle disintegration process. The effect of ultrasound does more to enhance the leaching rate for a comparatively higher particle size than for the lower particle size. This facet of acoustic cavitation can be taken as an advantage in reducing the need for fine grinding costs and particulate pollution associated with the grinding operation of the MgF_2 agglomerate (and also possibly uranium ore). In terms of energy consumption, the results are showing improvement by ultrasound induced cavitation in enhancing the leaching rate when compared to conventional stirring conditions.

Acknowledgment

The authors wish to acknowledge the funding of the Department of Atomic Energy, Govt. of India, under the project name DAE−KBE (Department of Atomic Energy−Centre for Knowledge Based Engineering, Project No. 47.01.12), for this collaborative research work.

Nomenclature

a_{av} = average specific surface area
A = component (uranium)
C_A = concentration of component (uranium) A
C_p = specific heat at constant pressure
D = diffusivity coefficient
D_t = diameter of the impeller
J_A = flux of component (uranium) A
L_d = amount of solute leached out (recovered)
L_o = total amount of leach solute (uranium) present in the MgF_2 particles
$L(t)$ = leached fraction
m = mass of the reaction mixture
N = number rotations per second (rps)
N_p = power number
n = integer of the infinite series
P_{diss} = dissipated power
r = radial distance from the MgF_2 particle center
r_o = initial MgF_2 particle radius
$t_{70\%}$ = time required for the70% of the uranium to leached out
t = time
V = leach acid solution volume
V_1 = volume of the MgF_2 agglomerate

Greek Letters

ρ = density of the solution
σ_{sd} = standard deviation of the droplet size

Appendix A: Energy Dissipation Calculation for Stirring Conditions

In the present work, for conventional stirring conditions, energy is dissipated in the form of a six-blade, 45°-pitch, down-pumping impeller. The impeller speed has been controlled by using a variable speed drive motor which is provided with a display to show the impeller rotational speed (rpm). Experiments have been performed at 600, 1000, 1500, and 1800 rpm.

A sample calculation for the energy dissipation rate at 1000 rpm (16.67 rps) under 10% (1.19 N) aqueous leach acid solution has been given here:

diameter of the impeller blade = 3.8 cm

composition of the slurry = MgF_2 (33.33% w/w), leach acid solvent (66.67% w/w)

density of MgF_2 = 1912.2 kg/m^3

density of water = 1000 kg/m^3

density of HNO_3 = 1420 kg/m^3

densities of different concentrations of HNO_3 with 50% (w/w) the solid loading of MgF_2 measured

density of an aqueous solution of 10% HNO_3 = ~1.222 g/mL (1222 kg/m^3)

density of an aqueous solution of 7.5% HNO_3 = ~1.214 g/mL (1214 kg/m^3)

density of an aqueous solution of 5.0% HNO_3 = ~1.205 g/mL (1205 kg/m^3)

power dissipation for 10% leach acid concentration at 1000 rpm speed = $P = N_p \rho N^3 D_t^5 = 2 \times 1222 \times 16.67^3 \times 0.038^5 = 0.897$ W (or) 8.97 kW/m^3

(power number (N_p) for the six-blade, down-pumping, 45°-pitch blade is taken as 2)

In the same way, the energy dissipation rate for the remaining rotational speeds 600, 1500, and 1800 are 1.91, 29.86, and 51.58 kW/m^3, respectively.

Appendix B: Energy Dissipation Calculation for Acoustic Cavitation Bath

The common problem in the sonochemical literature is that the power delivered to the system (as quoted by the manufacture) is mentioned but the actual power dissipated (P_{diss}) in the

reaction mixture is rarely reported. One of the most common methods of measuring (P_{diss}) is given by the equation[38]

$$P_{diss} = \left(\frac{dT}{dt}\right) mC_p$$

Where, m and C_p are the mass and heat capacity of the solvent, respectively, and (dT/dt) is the slope of the temperature of the reaction mixture versus the time it is exposed to ultrasonic irradiation. This equation is based on the use of calorimetry and assumes that all of the power entering the reaction mixture is dissipated as heat.

A separate experiment has been conducted to measure the dissipated power with 100 mL of water as a reaction mixture within the same reaction vessel. The mixture has been irradiated with ultrasound for 20 min, and the temperature rise has been measured to be 6 °C. Here, (dT/dt) = 0.005 °C/s ∴ the total dissipated power in 0.1 kg of water (P_{diss}) = 0.005 × 0.1 × 4184 = 2.092 J/s or W

energy dissipated per unit volume by ultrasonic irradiation = 20.92 kW/m^3

total energy dissipated during the experiment, i.e., (1000 rpm impeller speed along with the ultrasonic irradiation) = 8.85 + 20.92 = 29.77 kW/m^3

This energy of dissipation is obviously less than the energy dissipated through the conventional stirring process under 1800 rpm (51.58 kW/m^3).

Literature Cited

(1) Uranium and Uranium compounds. *Encyclopedia of Chemical Technology*, 3rd ed.; vol. 23, p 514.

(2) Thompson, L. H.; Doraiswamy, L. K. Sonochemistry: Science and Engineering. *Ind. Eng. Chem. Res.* **1999**, *38*, 1215.

(3) Ashokkumar, M.; Grieser, F. Ultrasound assisted chemical processes. *Rev. Chem. Eng.* **1999**, *15*, 44.

(4) Berlan, J.; Trabelsi, F.; Delmas, H.; Wilhem, A. M.; Petrignani, J. F. Oxidative degradation of Phenol in aqueous media using ultrasound. *Ultrason. Sonochem.* **1994**, S97−S102.

(5) Broeckaert, L.; Caulier, T.; Fabre, O.; Maerschalk, C.; Reisse, J.; Vandercammen, J.; Yang, D. H.; Lepoint, T.; Mullie, F. Quantitative homogeneous sonochemistry: scope and limitations. *Current trends in Sonochemistry*; Price, G. J., Ed.; Royal Society of Chemistry: Cambridge, 1992; vol. 8, p 25.

(6) Hamdaoui, O.; Naffrechoux, E.; Tifouti, L.; Petrier, C. Effects of ultrasound on Adsorption Desorption of *p*-chlorophenol on Granular Activated Carbon. *Ultrason. Sonochem.* **2003**, *10*, 109.

(7) Mason, T. J. *Practical sonochemistry: User's guide to Applications in Chemistry and Chemical engineering*; Ellis Horwood: Chichester, UK, 1991.

(8) Skauen, D. M. Problems in Ultrasonic Extraction on Pharmaceuticals. *Chem. Eng. Prog. Symp. Ser.* **1971**, *67* (109), 35.

(9) Schuller, B. S.; Yang, R. T. Ultrasound Enhanced Adsorption and Desorption of Phenol on activated carbon and Polymeric Resin. *Ind. Eng. Chem. Res.* **2001**, *40*, 4912.

(10) Breitbach, M.; Bathen, D.; Schmidt-Traub, H. Effect ultrasound on Adsorption and Desorption Processes. *Ind. Eng. Chem. Res.* **2003**, *42*, 5635.

(11) Hamdaoui, O.; Djeribi, R.; Naffrechoux, E. Desorption of Metal Ions from Activated Carbon in the Presence of Ultrasound. *Ind. Eng. Chem. Res.* **2005**, *44*, 4737.

(12) Swamy, K. M.; Rao, K. S.; Narayana, K. L. Murthy, J. S.; Ray, H. S. Application of ultrasound in leaching. *Min. Pro. Ext. Metal. Rev.* **1995**, *14*, 179.

(13) Narayana, K. L.; Swamy, K. M.; Rao, K. S.; Murthy, J. S. Leaching of metals from ores with ultrasound. *Min. Pro. Ext. Met. Rev.* **1997**, *16*, 239.

(14) Swamy, K. M.; Narayana, K. L. Intensification of leaching process by dual-frequency ultrasound, *Ultrason. Sonochem.* **2001**, *8*, 341.

(15) Pesic, B.; Zhou, T. Application of ultrasound in extractive metallurgy: sonochemical extraction of nickel. *Metall. Trans.* **1992**, *23B*, 3.

(16) Narayana, K. L.; Swamy, K. M.; Rao, K. S.; Murthy, J. S. Leaching of metals from ores with ultrasound. *Min. Proc. Ext. Met. Rev.* **1997**, *16*, 239.

(17) Orlov, A. I. *Izv. Vyssh. Uchebn. Zaved., Tsvetn. Metall.* **1975**, *1*, 85 (in Russian); *Chem. Abstr.* **1975**, *82*.

(18) Chizhikov, M. N.; Novitskii, B. G.; Fridman, V. M.; Khavskii, N. N.; Yu, R. Use of joint action of ultrasonic and electric field to improve leaching of metals. *Sb. Mosk. Inst. Stalii Spavov 77, 94* (in Russian); *Chem. Abstr.* **1975**, *82*, 173.

(19) Sukla, L. B.; Swamy, K. M.; Narayana, K. L.; Kar, R. N.; Panchanadikar, V. V. Bioleaching of Sukinda laterite using ultrasonics. *Hydrometallurgy* **1995**, *37*, 387.

(20) Polyukhin, P. I. *The use of Ultrasonics in Extractive Metallurgy Technicopy*; Stonehouse, UK, 1978.

(21) Tekin, T.; Tekin, D.; Bayramoglu, M. The effect of ultrasound on the dissolution kinetics of Phosphate rock in HNO_3. *Ultrason. Sonochem.* **2001**, *8*, 373.

(22) Tekin, T. Use of ultrasound in the dissolution kinetics of Phosphate rock in HCl. *Hydrometallurgy* **2002**, *64*, 187.

(23) Tarasova, I. I. Bio hydrometallurgical technologies. In *Proceedings of International Bioleaching Processing*; Torma, A. E., Wey, J. E., Lakshmanan, Eds.; TMS Min. Metals Mater. 1993; vol. 1, p 357.

(24) Rao, K. S.; Narayana, K. L.; Swamy, K. M.; Murty, J. S. Influence of ultrasound in ammoniacal leaching of a copper oxide ore. *Metall. Mater. Trans.* **1997**, *28B*, 721.

(25) Swamy, K. M.; Sukla, L. B.; Narayana, K. L.; Kar, R. N.; Panchanadikar, V. V. Use of ultrasound in microbial leaching of nickel from laterites. *Ultrason. Sonochem.* **1995**, *2*, S5−S9.

(26) Moholkar, V. S.; Warmoeskerken, M. M. C. G. Investigations in mass transfer enhancement in textiles with ultrasound. *Chem. Eng. Sci.* **2004**, *59*, 299.

(27) Braun, R. L.; Lewis, A. E.; Wadsworth, M. E. In-place leaching of primary sulfides ores: laboratory leaching data and kinetics model. *Metall. Trans.* **1974**, *5*, 1717.

(28) Levenspiel, O. *Chemical Reaction Engineering*; Wiley: New York, 1972.

(29) Pouchly, J. *Chem. Listy* **1958**, *52*, 996.

(30) Crank, J. *The Mathematics of Diffusion*; Oxford university press: New York, 1956.

(31) Vermeulen, T. Theory for Irreversible and Constant-Pattern Solid Diffusion. *Ind. Eng. Chem.* **1953**, *45*, 1664.

(32) Moholkar, V. S.; Warmoeskerken, M. M. C. G. Mechanistic Aspects and optimization of ultrasonic washing. *AATCC Rev.* **2002**, *2* (2), 34.

(33) Rayleigh, L.; Strutt, J. W. On the pressure developed in a liquid during the collapse of a spherical cavity. *Philos. Mag.* **1917**, *34*, 94.

(34) Gilmore, F. R. *The collapse and growth of a spherical bubble in a viscous compressible liquid*; Report No. 26-4, California Institute of Technology Hydrodynamics Lab: 1952.

(35) Tomita, Y.; Shima, A. On the behaviour of a spherical bubble and the impulse pressure in a viscous compressible liquid. *Bull. JSME* **1977**, *20*, 1453.

(36) Chen, Y.-S.; Christian Host, U.; Kunz.; Hoffmann, U. Design, modeling and performance of a novel sonochemical reactor for heterogeneous reactions. *Chem. Eng. Sci.* **1996**, *51*, 1837.

(37) Chen, Y.-S.; Christian Host, U.; Kunz.; Hoffmann, U. Method to determine surface area change rate in heterogeneous reaction under the influence of the ultrasound. In *Congress Proceedings*, World Congress on Ultrasonics, Berlin, 1995; No. 3, Vol. 2, p 675−678 (ISBN 3-9805013-0-2).

(38) Lorimer, J. P.; Mason, T. J.; Fiddy, K.; Enhancement of chemical reactivity by power ultrasound: an alternative interpretation of the hot spot. *Ultrasonics* **1991**, *29*, 338.

Received for review May 16, 2006
Revised manuscript received July 9, 2006
Accepted August 10, 2006

IE060599X